

## High electron mobility along the $c$ -axis in 4H-SiC

Ryoya Ishikawa, Masahiro Hara, Mitsuaki Kaneko, and Tsunenobu Kimoto

Dept. of Electronic Sci. & Eng., Kyoto University, Nishikyo, Kyoto, 615-8510, Japan

E-mail: [ishikawa@semicon.kuce.kyoto-u.ac.jp](mailto:ishikawa@semicon.kuce.kyoto-u.ac.jp)

### Abstract

The electron mobility along the  $c$ -axis in 4H-SiC with various donor concentrations ( $N_D$ ) of  $10^{15}$ – $10^{17}$   $\text{cm}^{-3}$  was investigated by Hall-effect measurement on n-type 4H-SiC (11 $\bar{2}$ 0) epitaxial layers in the temperature range from 296 to 573 K. We obtained a Hall electron mobility of 1108  $\text{cm}^2/\text{Vs}$  for  $N_D = 5.4 \times 10^{15}$   $\text{cm}^{-3}$  at room temperature, which is the highest electron mobility ever reported for SiC at room temperature, and the Hall electron mobility along the  $c$ -axis was about 1.2 times higher than that perpendicular to the  $c$ -axis. In addition, based on the temperature dependence of the resistivity, we concluded that the anisotropy of the drift mobility is mainly attributed to the anisotropy of the effective mass.

### 1. Introduction

The mobility is one of the most basic properties which determines characteristics of semiconductor devices. It is known that the mobility has anisotropy in hexagonal SiC [1–3]. Figures 1(a) and (b) show schematic structures of typical SiC vertical power devices, where the mobility along the  $c$ -axis determines the drift resistance because the current flow is along the  $c$ -axis. Although a number of studies have been conducted on measurements of the mobility in SiC, almost all of them investigate the mobility perpendicular to the  $c$ -axis using van der Pauw structure fabricated on SiC (0001) wafers shown in Fig. 1(c), and the mobility along the  $c$ -axis has not been well investigated. In this study, we measured the Hall electron mobility along the  $c$ -axis ( $\mu_{H,\parallel}$ ) and that perpendicular to the  $c$ -axis ( $\mu_{H,\perp}$ ) in the temperature range from 296 to 573 K using 4H-SiC (11 $\bar{2}$ 0) substrates. In addition, we discuss the anisotropy of the drift mobility based on the temperature dependence of the resistivity ( $\rho_{\perp}$ ,  $\rho_{\parallel}$ ).

### 2. Experiment

We fabricated Hall bar samples on n-type 4H-SiC (11 $\bar{2}$ 0) epitaxial layers with various donor concentrations ( $N_D$ ) of  $5.4 \times 10^{15}$ – $1.0 \times 10^{17}$   $\text{cm}^{-3}$ . A schematic illustration of the Hall bar structures is shown in Fig. 2. The intermediate p-type epitaxial layer was grown for electrical isolation of the n-type epitaxial layer from the n-type substrate. We fabricated two kinds of Hall bar structures on the sample, which are oriented along [0001] and [1 $\bar{1}$ 00] directions for measuring  $\mu_{H,\parallel}$  and  $\mu_{H,\perp}$ , respectively. Hall-effect measurement was performed on those structures, and the electron mobility and the resistivity were measured in the temperature range from 296 to 573 K.

### 3. Result and discussion

Figure 3 shows the Hall electron mobility versus the donor concentration at room temperature.  $\mu_{H,\parallel}$  was about 1.2

times higher than  $\mu_{H,\perp}$ , and a  $\mu_{H,\parallel}$  of 1108  $\text{cm}^2/\text{Vs}$  was obtained for  $N_D = 5.4 \times 10^{15}$   $\text{cm}^{-3}$ , which is the highest electron mobility ever reported for SiC measured at room temperature.

For calculation of the specific on-resistance (drift-layer resistance) for SiC devices,  $\mu_{\perp}$  has often been used. However,  $\mu_{\parallel}$  should be used instead of  $\mu_{\perp}$  because the current flow is along the  $c$ -axis in typical SiC vertical power devices. Figure 4 shows the drift-layer resistance of SiC device with an optimum punch-through (PT) structure [4] for voltage ratings of 3.3 and 6.5 kV (breakdown voltages of 4.0 and 7.8 kV) at room temperature calculated using  $\mu_{H,\perp}$  and  $\mu_{H,\parallel}$ , considering that  $\mu_{H,\parallel}$  is 1.2 times higher than  $\mu_{H,\perp}$ . The calculated drift-layer resistance was reduced from 5.6 to 4.6  $\text{m}\Omega\text{cm}^2$  for 3.3 kV devices and 25.6 to 21.4  $\text{m}\Omega\text{cm}^2$  for 6.5 kV devices by using  $\mu_{H,\parallel}$ .

Figure 5 shows the temperature dependence of the Hall electron mobility measured on the sample with  $N_D = 1.0 \times 10^{17}$   $\text{cm}^{-3}$ , where the  $\log \mu_H - \log T$  shows a linear relationship in the log-log plot. For other donor concentrations ( $N_D = 5.4 \times 10^{15}$ ,  $1.2 \times 10^{16}$   $\text{cm}^{-3}$ ),  $\mu_{H,\parallel}$  and  $\mu_{H,\perp}$  exhibited a similar tendency from 296 to 433 K.  $\alpha$  defined by  $\mu \propto T^{-\alpha}$  was determined as 2.92, 2.71, and 2.22 for  $\mu_{H,\parallel}$  and 2.87, 2.66, and 2.18 for  $\mu_{H,\perp}$  in the samples with  $N_D = 5.4 \times 10^{15}$ ,  $1.2 \times 10^{16}$ , and  $1.0 \times 10^{17}$   $\text{cm}^{-3}$ , respectively. The decrease in  $\alpha$  with increasing donor concentration is naturally expected due to the stronger effect of impurity scattering.

The relationship between the Hall electron mobility  $\mu_H$  and the drift mobility  $\mu$  is given by  $\mu_H = \gamma_H \mu$ , where  $\gamma_H$  is the Hall scattering factor. When the scattering process depends on crystal directions,  $\gamma_H$  has anisotropy and the anisotropy of  $\mu_H$  can differ from that of  $\mu$ . To discuss the anisotropy of  $\mu$  by excluding that of  $\gamma_H$ , we investigated the anisotropy of the resistivity  $\rho$ , which is directly related to  $\mu$  by  $\rho = 1/en\mu$ , where  $e$  and  $n$  are the elementary charge and the electron density, respectively. Figure 6 shows the ratio of  $\rho_{\perp}$  to  $\rho_{\parallel}$  versus the temperature from 296 to 573 K. We obtained the resistivity ratio  $\rho_{\perp}/\rho_{\parallel}$  of 1.20 and 1.08 for  $N_D = 5.4 \times 10^{15}$   $\text{cm}^{-3}$ , while 1.17 and 1.04 for  $N_D = 1.0 \times 10^{17}$   $\text{cm}^{-3}$  at 296 K and 573 K, respectively. The resistivity ratio becomes lower with elevating the temperature and as the donor concentration becomes higher. Considering the energy distribution of electrons in the conduction band, the number of electrons in the high energy should increase at higher temperature and with heavier donor concentration as shown in Fig. 7. Therefore, it is speculated that the anisotropy of the drift mobility is large near the conduction band minimum and becomes smaller in the higher energy region. The drift mobility  $\mu$  is related to the effective mass  $m^*$  and the average scattering time  $\langle \tau \rangle$  by  $\mu = e\langle \tau \rangle/m^*$ . Thus, the anisotropy of the drift mobility, in principle, originates from the anisotropy of  $m^*$  and/or  $\langle \tau \rangle$ . The ratio of  $m_{\perp}^*$  to  $m_{\parallel}^*$  ( $m_{\perp}^*/m_{\parallel}^*$ )

is 1.21, as calculated from the effective mass shown in Table I [5]. On the other hand, we obtained the ratio of the drift mobility  $\mu_{//}/\mu_{\perp} = 1.20$  (at room temperature,  $N_D = 5.4 \times 10^{15} \text{ cm}^{-3}$ ), which is close to the  $m_{\perp}^*/m_{//}^*$  ratio. This result implies that the anisotropy of  $m^*$  mainly contributes to the anisotropy of the drift mobility in 4H-SiC.

#### 4. Conclusion

In this study, we investigated the Hall electron mobility along the  $c$ -axis in 4H-SiC with various donor concentrations of  $10^{15}$ - $10^{17} \text{ cm}^{-3}$ . The mobility obtained in our work is essential for designing SiC vertical power devices.

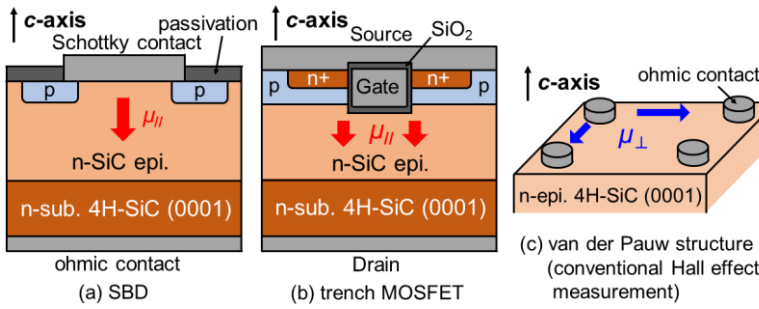


Fig. 1. Schematic illustrations of (a) Schottky barrier diode (SBD), (b) trench MOSFET, and (c) van der Pauw structure.

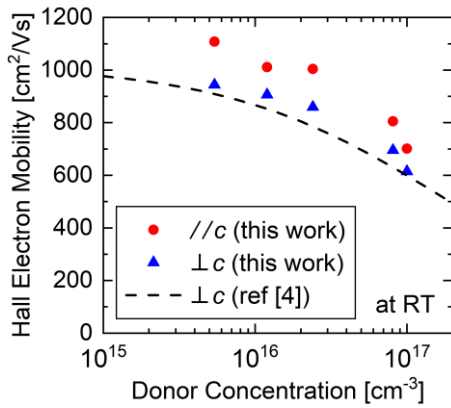


Fig. 3. Hall electron mobility versus donor concentration at room temperature.

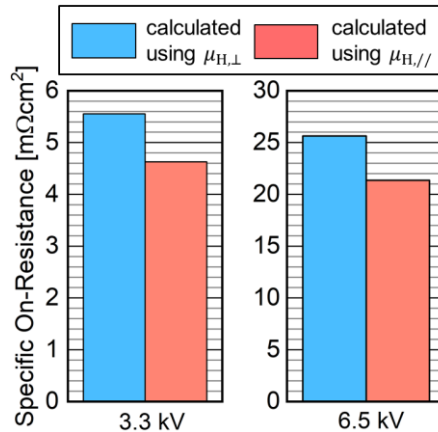


Fig. 4. Specific on-resistance (drift-layer resistance) of SiC devices for voltage ratings of 3.3 and 6.5 kV with a punch-through structure at room temperature.

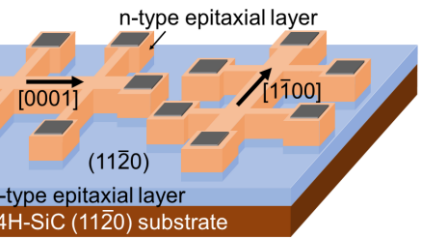


Fig. 2. Hall bar structures along  $[0001]$  and  $[1\bar{1}00]$  directions fabricated on an n-type epitaxial layer grown on a 4H-SiC  $(11\bar{2}0)$  substrate.

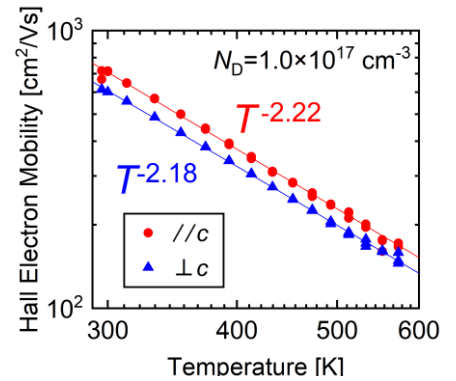


Fig. 5. Temperature dependence of the Hall electron mobility with a donor concentration of  $1.0 \times 10^{17} \text{ cm}^{-3}$ .

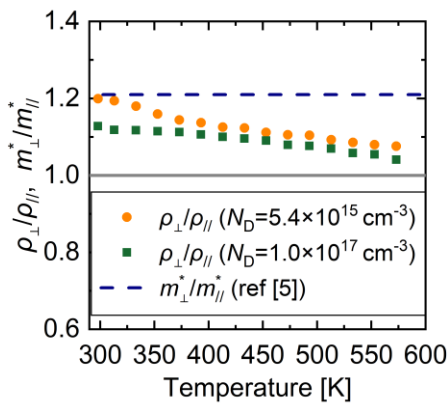


Fig. 6. Temperature dependence of the resistivity ratio ( $\rho_{\perp}/\rho_{//}$ ) with the donor concentrations of  $5.4 \times 10^{15}$  and  $1.0 \times 10^{17} \text{ cm}^{-3}$ . The broken line shows the ratio of the effective mass ( $m_{\perp}^*/m_{//}^*$ ) [5].

#### Acknowledgements

This work was supported by Council for Science, Technology and Innovation (CSTI), Cross-ministerial Strategic Innovation Promotion Program (SIP), “Next-generation power electronics/Consistent R&D of next-generation SiC power electronics” (funding agency: NEDO).

#### References

- [1] W. J. Schaffer *et al.*, *Mater. Res. Soc. Symp. Proc.*, **339**, 595 (1994).
- [2] M. Schadt *et al.*, *Appl. Phys. Lett.*, **65**, 3120 (1994).
- [3] T. Hatakeyama *et al.*, *Mater. Sci. Forum.*, **433-436**, 443 (2003).
- [4] T. Kimoto and J. A. Cooper, *Fundamentals of Silicon Carbide Technology* (Wiley, 2014).
- [5] N. T. Son *et al.*, in *Silicon Carbide – Recent Major Advances*, eds. W. J. Choyke *et al.* (Springer, 2004), p.437.

Table I. Electron effective mass in 4H-SiC [5].

$m_{ML}(=m_{//})$	$m_{MF}$	$m_{MK}$	$m_{\perp}$	$m_{\perp}/m_{//}$
$0.33m_0$	$0.58m_0$	$0.31m_0$	$0.40m_0$	<b>1.21</b>

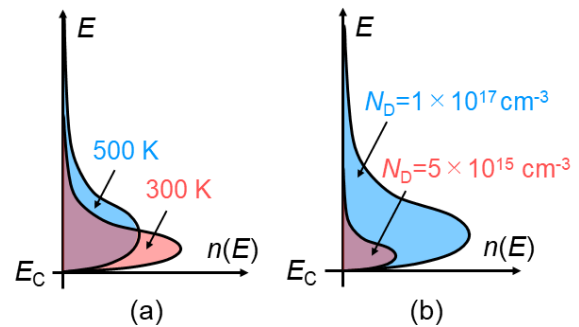


Fig. 7. Schematic diagrams of the energy distribution of electrons (a) at different temperatures and (b) for different donor concentrations.